Guidance, Navigation, and Control and Co-located Conferences
August 19-22, 2013, Boston, MA
AIAA Guidance, Navigation, and Control (GNC) Conference

Vision-Based Relative Navigation and Control for Autonomous Spacecraft Inspection of an Unknown Object

Dehann Fourie[1], Brent E. Tweddle[2], Steve Ulrich[3], and Alvar Saenz-Otero[4]
Massachusetts Institute of Technology, Cambridge, Massachusetts, 02139

This paper describes a vision-based relative navigation and control strategy for inspecting an unknown and non-cooperative object in space using a visual-inertial system. The proposed inspection spacecraft system relies solely on a calibrated stereo camera and a 3-axis gyroscope to maintain a safe inspection distance while following a circle trajectory around the object. The navigation system is based on image processing algorithms which extract the relative position and velocity between the inspector and the object, and a simple control approach is used to ensure the desired range and bearing are maintained throughout the inspection maneuver. Hardware implementation details of the VERTIGO Goggles system are provided, and design considerations related to the addition of the stereo camera system and associated processor unit to the SPHERES satellites are discussed. Computer simulation results, and experiments conducted aboard the International Space Station during Expedition 34 are reported to demonstrate the performance and applicability of the proposed hardware and related navigation and control systems to inspect an unknown spacecraft.

I. Introduction

Spacecraft robotic inspection is an important technological capability that enables a large number of different types of spacecraft proximity operations, including International Space Station (ISS) supply, and on-orbit servicing of spacecraft.[1] However, because of the very nature of on-orbit servicing missions, the object spacecraft might not be fully cooperative. Additionally, it may be freely tumbling due its intrinsic design, or to various mechanical failures or fuel depletion.[2] Moreover, during close proximity operations, the safe time frame to react to anomalies is reduced. For example, when the object spacecraft is tumbling, the likelihood of collisions with solar panels or antennas is greatly increased. To address these problems, it is required that the servicer spacecraft relies on an accurate navigation and control system to autonomously determine and control its relative states with respect to the object. Recently, a number of theoretical research studies have addressed the problem of spacecraft navigation for proximity operations. In particular, Hablani[3] proposed a relative navigation technique for autonomous rendezvous and docking using an integrated sensor suite onboard an active chaser satellite, which comprises an imaging sensor, a laser range finder, the space-integrated Global Positioning System and inertial navigation system, and a star tracker. However, it is well known that GPS and GPS-like signals are susceptible to interference and jamming.

For this reason, GPS-less navigation systems for autonomous vehicles is currently an active area of research. Particularly, vision-based relative navigation systems are expected to play an important role in future missions, since, compared to other navigation technologies (e.g LIDAR, laser range finder, GPS, ground-based measurements), computer vision offers several advantages, such as low power and volume requirements.[4] For example, Linares et al.[5] developed an approach for the relative attitude determination between two autonomous vehicles based on line-of-sight measurements between both vehicles and a third cooperative object. References 6

[1]Visiting PhD Student, Space Systems Laboratory, Department of Aeronautics and Astronautics, Computer Science and Artificial Intelligence Laboratory, 77 Massachusetts Avenue.
[2]PhD Candidate, Space Systems Laboratory, Department of Aeronautics and Astronautics, 77 Massachusetts Avenue. Student Member AIAA.
[3]Postdoctoral Associate, Space Systems Laboratory, Department of Aeronautics and Astronautics, 77 Massachusetts Avenue. Member AIAA.
[4]Research Scientist, Space Systems Laboratory, Department of Aeronautics and Astronautics, 77 Massachusetts Avenue. Senior Member AIAA.

and 7 report on-the-ground laboratory experimentations of vision-based relative navigation between a chaser spacecraft and a target object equipped with different fiducial markers (Light Emitting Diodes in the prior study, and four point correspondences in the latter work). In the past, vision-based navigation systems using fiducial markers have been successfully validated in different space missions. Jointly-developed by the Canadian Space Agency and NEPTEC, the Space Vision System used cameras to monitor a pattern of special target dots placed on the object to be tracked. As the object moved, the system tracked the changing position of the dots, calculated the location and orientation of the object, and presented this information to the operator in the form of both graphical and textual cues. This information was namely used to position and orient a payload using Canadarm2, or to join two objects as in the case of Space Station assembly.[8] On DARPA's Orbital Express mission, the Advanced Video Guidance Sensor was used for docking between two spacecraft. A laser diode was used to illuminate a retro-reflective visual target that was processed by machine vision algorithms to determine the relative position and orientation between the two spacecraft.[9]

However, when the target object has an unknown geometry and no fiducials, such vision systems cannot be employed and more advanced technologies are required. Therefore, to address the problem of autonomous vision-based relative navigation and control to perform an inspection maneuver of an unknown object, the Massachusetts Institute of Technology (MIT) developed, under DARPA's funding, and in collaboration with Aurora Flight Sciences, the United States Air Force Space Test Program, and NASA, the *Visual Estimation for Relative Tracking and Inspection of Generic Objects* (VERTIGO) ISS-based research experiment. This space robotics experimental testbed enables research and development of computer vision-based navigation and mapping algorithms capable of achieving two main objectives: (1) performing relative navigation by relying solely on camera hardware and inertial sensors, and (2) building a three-dimensional map of another unknown, non-cooperative object and performing relative navigation solely by reference to this three-dimensional model. Building upon the experience gained under the United States Naval Research Laboratory's Low Impact Inspection Vehicle (LIIVe) program,[10,11] the VERTIGO program designed, built, test and launch to the ISS a hardware upgrade to the existing Synchronized Position Hold Engage and Reorient Experimental Satellites (SPHERES) laboratory facility to test these algorithms.

This paper addresses the first phase of the VERTIGO program, i.e. the problem of performing an autonomous robotic vision-based circumnavigation maneuver about an unknown object by relying solely on computer vision and inertial sensors. To achieve this, the proposed relative navigation and control scheme uses relative position measurements provided by calibrated stereo monochrome cameras, along with angular rates from a 3-axis gyroscope mounted on the inspecting spacecraft, to ensure that it maintains a body-fixed orientation with respect to the object.

This paper is organized as follows: Section 2 provides an overview of the relative navigation and control approach. Section 3 describes the existing SPHERES facility along with the stereo cameras and associated processor unit (referred to as the VERTIGO Goggles) required to enable vision-based navigation research. Section 4 outlines software modifications required to accommodate center of mass offset location due to the addition of the VERTIGO Goggles to the SPHERES satellite. In Section 5, the image processing strategy employed to provide relative measurements is described. Section 6 presents and discusses numerical simulation results, and Section 7 presents on-orbit results of experiments conducted aboard the ISS during Expedition 34 by Commander Kevin Ford. To the best of our knowledge, this was the first time a fully-autonomous robotics vision-based navigation strategy was demonstrated in space with an unknown spacecraft.

II. Circumnavigation Control Approach

The proposed relative navigation and control approach intends to accomplish an autonomous circumnavigation trajectory about an unknown object based only on visual-inertial information. This proposed control approach is illustrated in Fig. 1. Throughout the inspection trajectory, the inspector spacecraft must always point its body-frame x-axis towards the object, to maintain the object within its field of view. To do so, the inspector satellite control input torque is obtained with a simple linear attitude control law of the form:

$$\tau = k_{\omega}\omega_{e} \tag{1}$$

where τ and k_{ω} respectively denotes the control input torque vector, and the angular rate control gain matrix, and where the angular rate control error, denoted by ω_{e}, is defined as

$$\omega_{e} \triangleq \omega_{d} - \omega_{m} \tag{2}$$

with $\omega_m = \begin{bmatrix} \omega_{mx} & \omega_{my} & \omega_{mz} \end{bmatrix}^T$ denoting the inspector angular rate, as measured directly by its body-mounted gyroscopes, and with ω_d given by

$$\omega_d = \begin{bmatrix} 0 & 0 & \omega_{dz} \end{bmatrix}^T \tag{3}$$

such that the angular rate about the body axis perpendicular to the plane of inspection (z axis in this case) is controlled to a constant value, while the other two angular rate components (x and y) are regulated to zero.

As the spacecraft rotates with a constant angular rate, the position of the target object will drift to one side in the field of view of the camera system. To ensure that the target is maintained in the center of the cameras field of view, the inspector spacecraft is translated by non-rotational forces until the pan error distances have been regulated to zero. Simultaneously, the relative position to the target spacecraft, which is obtained from the camera system and through image processing algorithms (see Section V) is controlled to a desired value along the x-axis of the body frame, to follow an inspection trajectory with a constant radius. The control input force is given by the following proportional-derivative (PD) translational feedback control law

$$f_{FB} = k_p r_e + k_d \dot{r}_e \tag{4}$$

where f_{FB}, k_p, and k_d, denotes the control input force vector, and the proportional and the derivative control gain matrix, respectively, and where the Cartesian position control error, denoted by r_e, is defined as

$$r_e \triangleq r_d - r_m \tag{5}$$

where $r_m = \begin{bmatrix} x_m & y_m & z_m \end{bmatrix}^T$ denotes the relative Cartesian position, which is measured by the camera system, and where $r_d = \begin{bmatrix} x_d & y_d & z_d \end{bmatrix}^T$ denotes the desired relative Cartesian position, as commanded by the user. Since it is desired to maintain a constant, safe distance along the line of sight of the cameras between both spacecraft as the inspector follows a circumnavigation trajectory, r_d and $\dot{r}_d$ were selected as

$$r_d = \begin{bmatrix} x_d & 0 & 0 \end{bmatrix}^T \quad \text{and} \quad \dot{r}_d = \begin{bmatrix} 0 & 0 & 0 \end{bmatrix}^T \tag{6}$$

In other words, the visual navigation system measures the panning offset as the inspector satellite rotates off target. The translational controllers then react by nulling the pan offset of the target in the field of view.

Once the inspector satellite achieves steady state rotation rate, that is, with the attitude control law (1), and constant tangential velocity with control law (4), a feedforward force term, denoted by f_{FF} is used to compensate for the centripetal acceleration, as follows

$$f_{FF} = m r_d \left| \omega_d \right|^2 \tag{7}$$

The resulting control input force is then given by

$$f = f_{FB} + f_{FF} \tag{8}$$

Both control inputs are combined together by a thruster mapping function that calculates, at a frequency of 1 Hz, the firing time of each of the 12 individual thrusters, denoted by u_n. Finally, the control software cycle opens and closes the solenoid valve-actuated thrusters according to their respective firing times. The maximum firing time is set to 400 ms per 1Hz cycle. The complete block diagram of the proposed navigation and control strategy is shown in Fig. 1.

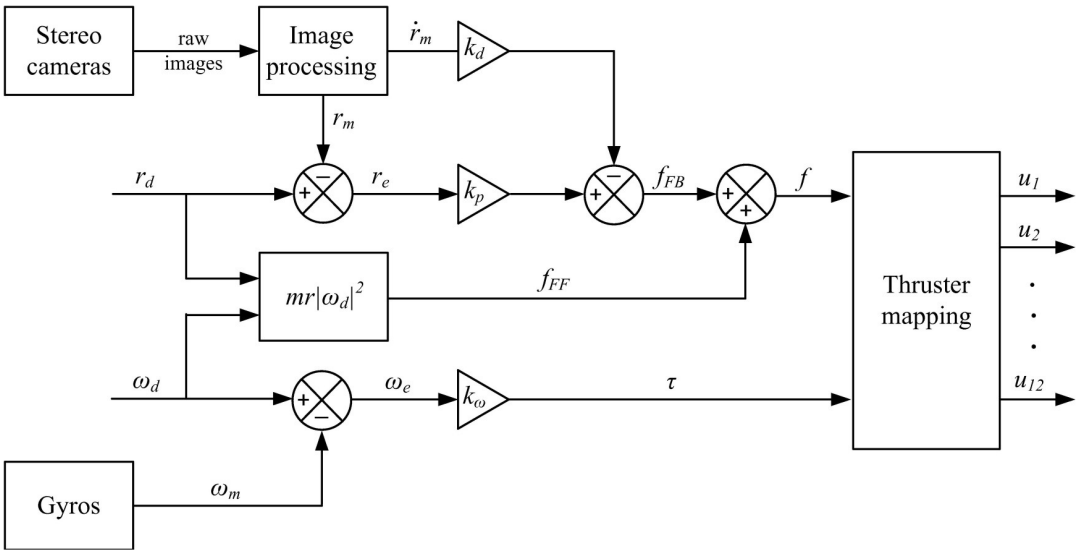

Fig 1. Vision-based control strategy block scheme implementation diagram.

III. Hardware Design and Description

This section gives an overview of the existing SPHERES research facility and of the recently-developed VERTIGO Goggles that enable vision-based navigation research.

A. SPHERES

From 1999 to 2000, as part of a capstone design course at the MIT Space Systems Laboratory, the SPHERES nanosatellite testbed was developed to provide researchers with an experimental laboratory to validate autonomous guidance, navigation, and control (GN&C) algorithms for advanced space mission scenarios, such formation flying, and rendezvous and docking. The SPHERES facility consists of three nanosatellites, which can autonomously maneuver in a 6-DOF environment. The testbed includes both a ground and a space segment, each able to operate independently of one another. The testbed is primarily designed to operate inside the ISS microgravity environment to represent the realistic dynamics of spacecraft in close proximity operations, but it can also operate onboard NASA's reduced-gravity aircraft as well as in a 3-DOF environment on a large flat floor or on a laboratory air table. The algorithms are first validated in a high-fidelity MATLAB simulation environment. After experimental testing with the SPHERES hardware in the 3-DOF air-bearing facility at the MIT, the GN&C software is packaged and sent to NASA for testing on the ISS. The software (written in C) consists of a series of modules, each accomplishing a specific task (navigation, control, thruster management, and maneuver sequencing). The modularity of the code allows flexibility in designing an experiment through the selection of different combinations of modules. Inheritance between experiments and reuse of previously validated software modules increases the robustness of the code and enables incrementally mature GN&C technologies.

Each of the three SPHERES satellites is self-contained and is equipped with 3-axis gyroscopes and accelerometers, 12 cold gas thrusters and a CO_2 tank for propulsion, AA batteries for power, as well as two low-power RF links to communicate with the other satellites and with an ISS laptop throughout a test session (for real-time monitoring and post-processing analysis. The navigation system employs time-of-flight data of ultrasonic signals emitted from external transmitters and received by microphones on the satellites In other words, the baseline measurement is the time that the ultrasonic signal takes to travel from a given transmitter mounted at a known location in the test volume to a given microphone (receiver) located on the satellite. Given that there are 5 beacons mounted on the walls and 24 microphones on each satellite, there is a potential of 120 measurements per satellite per measurement cycle. The time-of-flight data can be converted to range data using the known speed of sound in the ISS. At a 5Hz frequency, these data are then merged with the 3-axis gyroscope measurements into an extended Kalman filter (EKF) to compute the 6-DOF state vector (position, velocity, quaternion, and angular rate). The resulting precision on the estimates is a few millimeters in position and approximately 1 deg in attitude in most of the testing volume. More details about the SPHERES navigation system can be found in Ref. 12.

B. VERTIGO Goggles

The VERTIGO Goggles are an upgrade to the SPHERES satellites that enable computer vision-based navigation algorithms to be developed, implemented and tested in a micro-gravity environment aboard the ISS. They include a pair of monochrome stereo cameras, an embedded Ubuntu Linux computer, a Wi-Fi card, lithium batteries and the associated electromechanical hardware to operate safely in the ISS environment. Two VERTIGO Goggles were launched to the ISS in October of 2012 and were successfully used by astronaut Thomas Marshburn for the first time in February 2013. A checkerboard camera calibration target was launched with the Goggles and a re-calibration using OpenCV was successfully performed while on orbit. Table 1 provides the specifications of the VERTIGO Goggles hardware.

Table 1. VERTIGO Goggles hardware specifications

Characteristic	Description
Cameras	Two monochrome 640 x 480 CMOS cameras
Lenses	Wide angle 2.8 mm f/1.3 CCTV lens with manual iris and focus
Lighting	Two 617 nm, 137 lm exposure synchronized LEDs
Computer	VIA PicoITX EPIA-P830: 1.2 GHz x86 Via Nano Processor 4GB RAM, 1 MB L2 Cache, SSE3
Operating System	Linux Ubuntu 10.04 server with OpenCV 2.3.1 and Intel IPP pre-installed
Storage	Two 64GB Flash SATA drives
Wi-Fi	802.11n USB
Power Consumption	17 W (Idle) 23 W (Typical) 30 W (max)
Battery	Nikon EN-EL4a 11.1V, 2500 mAh (approx. 90 min runtime)
Mass	1.750 kg (with battery), 1.588 kg (without battery)

The Goggles can be expanded by attaching through a single 1Gbps Ethernet port, two USB 2.0 ports, the 802.11n Wi-Fi connection or by removing the optics mount (4 thumb-screws) and mounting directly to a 50 pin power and data connector.

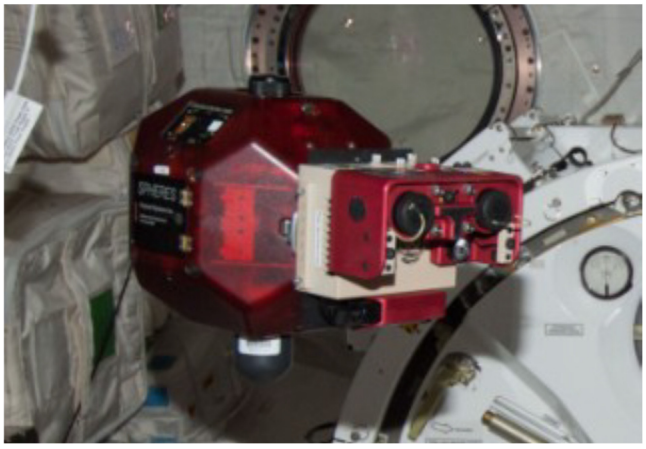

Fig 2. A SPHERES satellite equipped with the VERTIGO Goggles operating aboard the International Space Station.

IV. Actuation and Reconfigurable Thrusting

The original SPHERES satellites were designed to have the center of mass and geometric center of the satellite coincide. While this is an expected design choice, the addition of extra mass to the satellite with the VERTIGO extension moves the center of mass away from the geometric center of the satellite. Furthermore the addition of asymmetric mass to the system complicates the rotational and translational axes of the satellite in a different way. The original control software for SPHERES relied on the assumption of symmetrical physical properties. The addition of the goggles hardware has required several more significant changes to the control software. To illustrate this, consider the numerical values pertaining to the physical hardware used. Table 2 presents physical parameters which are relevant to the discussion.

Table 2. VERTIGO Goggles hardware specifications

Parameter	Unit	SPHERES	VERTIGO
Mass			
m	kg	4.25	1.75
Inertia			
I_{xx}	kg m^2	0.0241	0.006
I_{yy}	kg m^2	0.0234	0.038
I_{zz}	kg m^2	0.0201	0.038

The Goggles hardware is only around 27 % of the total system mass, yet it contributes more than 63 % of the inertia. The center of mass of the total system is moved by 25 mm from the original satellite geometric center. More specifically, the center of mass location offset vector in the satellite body frame is

$$R_{GC \to CM} = [0.025 \quad 0 \quad 0.003]m \tag{9}$$

This translates into a center of mass disturbance of around 11 % the original satellites longest dimension. This change is separated from the satellite control laws through the use of a *reconfigurable thruster mapping strategy*, which is discussed below. The disturbance to the rotational dynamics of the vehicle is affected to a much larger extent.

Addition of the 1.75 kg VETIGO Goggles component at a lever arm distance of 0.168 m (satellite geometric center to VERTIGO Goggles center of mass), increases the original rotational inertia by more than 170 % along the y and z body reference frame axes. The x axis is not perturbed as significantly, only 27 %. The drastic and asymmetric perturbation to the rotational inertial properties complicates the control requirement of the SPHERES satellites. The problem was further worsened in that the original SPHERES control software architecture has been developed over a period of nearly a decade with mostly symmetrical inertia properties.

As mentioned earlier, the SPHERES satellites actuation is achieved through twelve CO_2 gas thrusters evenly distributed around the satellite body. The thrusters are driven from a common pressurized gas tank through a regulator. Thruster impulses are assumed to be consistent, and varying forces are achieved through pulse width modulation. A thruster mapping algorithm is used to convert body relative forces and torques to thruster on and off firing times. Various combinations of these thruster firing times are used to achieve full six degree of freedom actuation. The mapping between thruster firing times and body forces and torques is described as follows:

$$\begin{bmatrix} f \\ \tau \end{bmatrix} = A \begin{bmatrix} u_1 \\ u_2 \\ \vdots \\ u_{12} \end{bmatrix} \tag{10}$$

where, A is a 6×12 matrix that defines the relation between individual thruster forces and the forces and torques to the center of mass of the satellite. The mapping is generally hard-coded as the inertia tensor and mass properties of the satellite was expected to remain constant over the course of the SPHERES test session. Indeed, thus far the SPHERES satellites have operated under the constant center of mass assumption.

The addition of the VERTIGO Goggles hardware moves the center of mass position of a SPHERE satellite as described by Eq. (9). Fig. 3 conceptually shows how the translational thrusters of the SPHERES satellite need to fire in order to maintain rotation free translation actuation, allowing stable circumnavigation around the target object. Notice how the mass asymmetry translates into asymmetric thruster firings.

Future experiments related to SPHERES and VERTIGO are expected to include robotic manipulation tasks, which involve various center of mass variations during a flight operations of the satellite. A dynamic reconfigurable thrusting capability will allow future experiments to vary the center of mass location of the system, as the satellite interacts with or manipulates its environment in real-time. This capability – together with visual-based navigation and autonomous volumetric object reconstruction – makes robotic operations such as maintenance or assembly of objects more achievable.

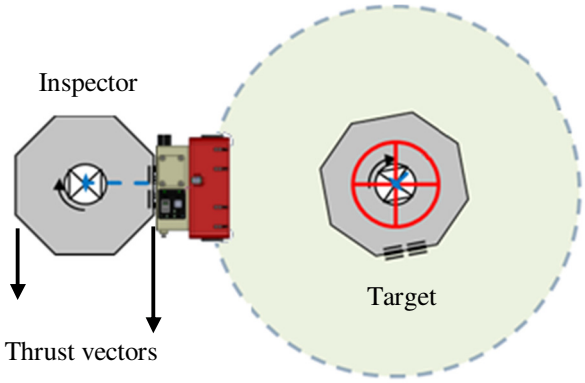

Fig 3. Pictorial showing different thrust requirements from the SPHERE satellite with offset center of mass to circumnavigate around the target while maintaining the line of sight vector.

Building, in part, upon a reconfigurable thruster mapping technique from previous work at the MIT Space Systems Laboratory,[13] a real-time reconfigurable thrusting computation capability was developed and integrated for the VERTIGO experiments. The developed thruster mapping algorithm dynamically adjusts firing time asymmetry for each thruster to accommodate changes in center of mass of the satellite. Although a fully dynamic reconfigurable mixing strategy is not required for VERTIGO-SPHERES operations, the capability has been established for expected for future SPHERES operations involving dexterous manipulation arms. The matrix A, from Eq. (10) is dynamically modified according to the varying system parameters. The three dimensional force impulse (N/s) of each of the twelve thrusters is hard-coded in a 3 × 12 input force matrix, $\hat{M}_b$. Thereby, the directionality of the input force is described in the row wise unit direction vectors in the $\hat{M}_b$ matrix, as follows

$$\hat{M}_b = \begin{bmatrix} f_{x1} & \cdots & f_{x12} \\ f_{y1} & \cdots & f_{y12} \\ f_{z1} & \cdots & f_{z12} \end{bmatrix} \tag{11}$$

The three dimensional relative position of the thrusters is described in a similar matrix, R_0. The translational vector for each thruster is described in terms of a particular reference point inside the satellite. Conventionally this has been the geometric center of the SPHERES satellite, which was assumed to coincide with the center of mass of the satellite. A second offset vector, geometric center location to the center of mass location, is now defined to compensate for changes in center of mass position and is denoted by $R_{GC \to CM}$. The new thruster position matrix is dynamically computed:

$$R_{CM} = R_0 - R_{GC \to CM} \tag{12}$$

The torque about the center of mass of the satellite, denoted τ_{CM} is computed, column by column, for each thruster through a standard cross product

$$\tau_{CM}^T = R_{CM}^T \times \hat{M}_b^T \tag{13}$$

The thruster force matrix $\hat{M}_b$ and computed torque mappings are stacked to form the new *A* matrix:

$$A = \begin{bmatrix} \hat{M}_b \\ \tau_{CM} \end{bmatrix} \tag{14}$$

Since the thrusters allow full six degree of freedom actuation, A is full rank, the pseudo inverse of A can be used to solve for the inverse of Eq. (10).

$$A' = A^T A \tag{15}$$

Cholesky decomposition is used to solve for the inverse as part of the satellite control cycle computations

$$\begin{bmatrix} u_1 \\ u_2 \\ \vdots \\ u_{12} \end{bmatrix} = \left(A'\right)^{-1} A^T \begin{bmatrix} f \\ \tau \end{bmatrix} \tag{16}$$

The reconfigured force per thruster is obtained. The required firing time for each thruster u_n is computed by dividing the required force with the known thruster impulse per time thrust value. Thruster variation and misalignments is accommodated through proper definition of $\hat{M}_b$.

The SPHERES satellites restrict the minimum and maxi/mum firing times for each thruster. In the event of a thruster firing time exceeding the maximum allotted time, all thrust firing times are scaled down, such that the maximum firing time is within the allowable firing time limit.

V. Image Processing for Relative Navigation

In order for a spacecraft to inspect a target object, it must utilize an estimation algorithm that is capable of determining the relative pose of the inspecting vehicle so that its planning and control system can maintain a safe distance while keeping the target object in view. A typical method to achieve this would be to track feature points on the object and use a visual odometry algorithm.[14–17] Visual odometry algorithms would solve for the relative position and orientation between the target and the inspector, thereby estimating a total of six degrees of freedom. One problem with this approach occurs if the target is tumbling or spinning. A visual odometry algorithm would assume that the target is static and estimate a circular trajectory for the motion of the inspector even if the inspector spacecraft was stationary in inertial space. This type of estimate would be problematic if no other reference to an inertial reference frame was considered; due to the fact that a command to *station-keep* with the target object would actually have the inspector spacecraft follow a circular trajectory and expending considerable fuel in the process. This is the primary reason why a visual odometry approach was not considered in this work.

Alternatively, the ability to estimate the target object's center of mass would provide a measurement that does not vary as the target object tumbles or rotates. However, the center of mass of the target object is unobservable from a single pair of stereo images. Instead, an estimate of the center of geometry of the visible portion of the target object is used as an approximation of the center of mass. Clearly the center of geometry will be an inherently biased estimate of the center of mass, and may in fact vary as the target object spins. However, if a lower accuracy navigation and control system is acceptable for an application, this type of approach would be largely independent of tumbling and spinning motions. The image processing strategy developed is described in the remainder of this section.

The first step is to capture a set of raw stereo images, shown in Fig. 4. It is important to note that when observing a tumbling or spinning object, both stereo cameras must be precisely synchronized to capture images at the same time. Additionally, the exposure time must be set low enough that there is very little motion blur. Both of these requirements are met by the VERTIGO Goggles hardware.

The second step is to remove any lens distortions and to adjust for any misalignment between the image sensors and lenses as well as between the two image sensors themselves. This is achieved using the publically available OpenCV library.[18] The result of this rectification and un-distortion step is shown in Figure 5.

Fig. 4. Raw stereo images prior to un-distortion.

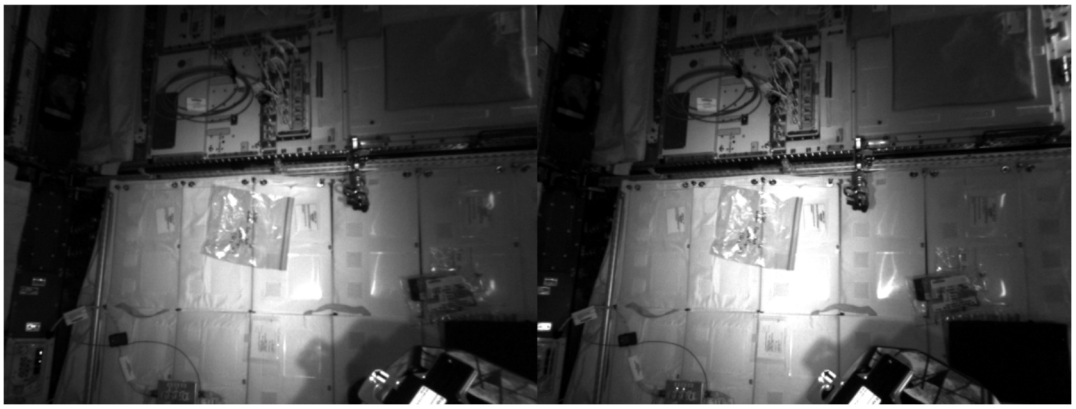

Fig. 5. Stereo images after un-distortion.

The third step is to compute a stereo disparity map. Since it is likely that there will be other objects and clutter in the background when the tests are performed aboard the ISS, it is useful to filter out parts of the stereo disparity map points that are too far away. OpenCV's stereo block matching algorithm was originally considered as a method to compute the disparity map, due to its speed and simplicity. However, since block matching is a local disparity algorithm, the resulting disparity map was often sparse and the field of view was restricted. Instead, the algorithm by Geiger et al.[19] was used. This algorithm uses belief propagation with a prior obtained using Delaunay triangulation of matched Sobel features to compute a global disparity map with relatively low computational cost. Once the disparity map is computed, the remaining points are triangulated to compute a three dimensional point cloud. The mean value of this point cloud is calculated and used as the estimate for the geometric center of the target object, which is an inherently biased estimate of the center of mass. The velocity is computed using a first order difference.

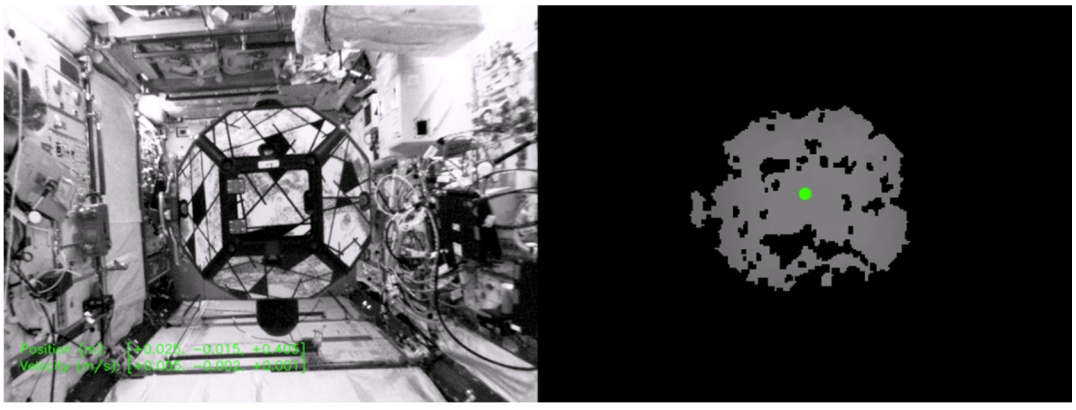

Fig. 6. Stereo disparity map. The green dot indicates the location of the center of geometry.

In Fig. 6, the left-hand image shows the original image from the left camera while the right-hand image shows the thresholded stereo disparity map, where a green dot is overlaid at the location of the geometric center and the position and velocity of this point, in meters and meters per second, respectively, are shown as green text overlaid on the right hand image. Note that these measurements represent the relative position and velocity between the geometric center of the object and the origin of a reference frame centered at the focal point of the left camera.

Additionally, ground experiments revealed that although there can be a sizable rotation that occurred between two images (in the case of a rotating target), the position and velocity estimates overlaid in the two images show that the estimate only changed by a few millimeters and millimeters per second. This supports the conclusion that although this type of estimator is inherently biased, it has a high repeatability that will not cause the inspector spacecraft to expend an overly large amount of fuel due to tracking sensor noise. Additionally, it is helpful to note that a tape measure was used in a ground experiment to measure to the geometric center/rotation of a target object, and it showed that the vision-based estimate was accurate to within one or two centimeters for this particular case.

VI. Simulation Results

Simulation of the SPHERES and VERTIGO system was developed and used to evaluate the flight software before testing aboard the ISS. The simulation evaluation described here was built on the existing SPHERES MATLAB® simulation environment, adding VERTIGO specific features. Specific satellite properties, including changes in mass, center of mass, center of mass to ultrasonic receive locations and inertia tensor were modified. Additional call back functions, which would imitate the software processes on the VERTIGO hardware and was also included into the simulation environment. The following questions may be asked to establish the capability and robustness of rotational inspection around an unknown object, based on the techniques proposed above: (1) can the visual navigation system, together with the inertial sensors be effectively used to navigate relative to the unknown object?, and (2) is a SPHERES equipped with VERTIGO Goggles able to follow a stable and controlled path during inspection maneuvers?

To gather initial results and information relevant to answering these questions, numerical simulations were conducted, and results are presented in Figs. 7 to 9. The selected inspection scenario consists in the following: the test starts with the inspector satellite at a short distance from the object, and with the object in the field of view. The inspector satellite approaches and maintains predefined relative distance from where the visual-inertial circumnavigation maneuver is initiated. Rotation around the object is achieved by changing the desired angular rate in the inspector yaw axis to a non-zero value, as discussed in Sec. II. The target then starts to drift to the side of the camera view. The visual feedback loop registers this offset and commands a control translational force to maintain the target in the field of view. The translational and rotational dynamics of the inspector are controlled independently, for which the reconfigured thruster mapping strategy accounts asymmetric mass distribution.

Figure 7 depicts the three dimensional trajectory around the unknown object and Fig. 8 illustrates the position and velocity states for the inspector satellite with respect to an inertial reference frame. As shown in Fig. 8, x and y positions both describe a sinusoid as the inspector spacecraft moves around the object satellite. The next important criterion of the controller is the ability to maintain the commanded range from the target object. Figure 9 shows that the inspector maintains a range of 0.68 m indicated by the solid line, which corresponds to the desired range, indicated by the dashed line. These results predict good control authority on range.

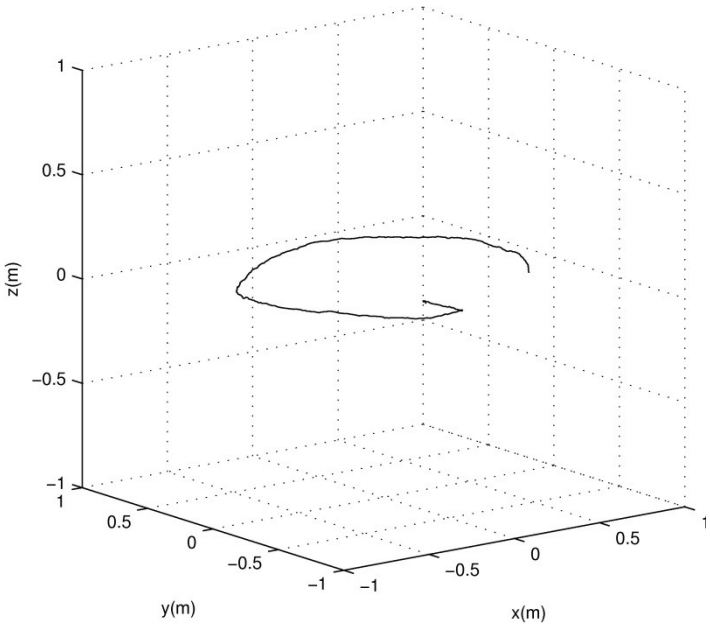

Fig. 7 Simulation results: 3D visualization of the inspector spacecraft circumnavigation trajectory.

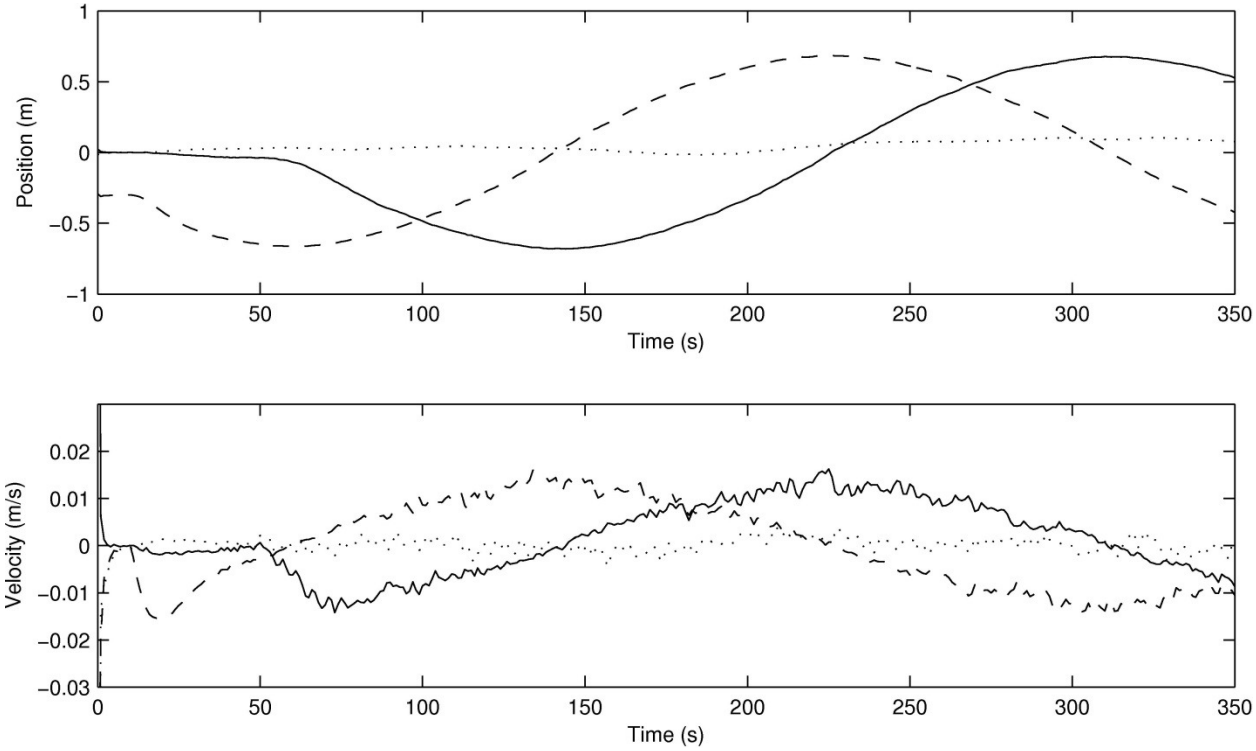

Fig. 8 Simulation results: inspector spacecraft position and velocity. The solid lines, the dashed lines and the dotted lines correspond to the x, y and z axis, respectively.

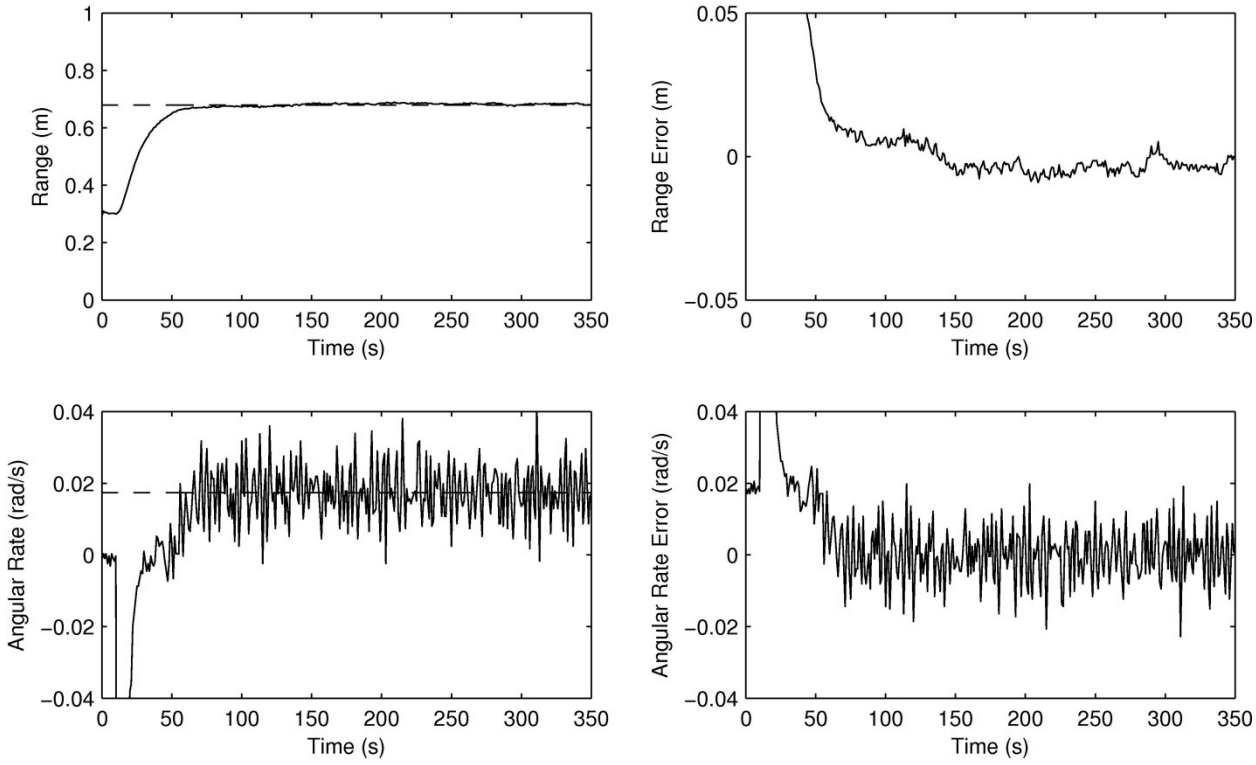

Fig. 9 Simulation results: range to target spacecraft and angular rate of the inspector spacecraft. The solid lines correspond to the actual values, and the dashed lines correspond to the desired values.

VII. ISS Flight Results

VERTIGO was operated on 26 February 2013 and 12 March 2013, during ISS Expedition 34, by Flight Engineer Thomas Mashburn and Commander Kevin Ford, respectively. On-orbit operations consisted of installing the VERTIGO hardware to the SPHERES hardware, adding texture stickers to the target SPHERES, performing on-orbit calibration of the cameras, uploading the navigation and control code into the flight hardware, executing the code, and downloading data to the station laptop for post-processing analysis of the data.

The objective of the first day of operation consisted mainly in performing an initial checkout of the integrated VERTIGO hardware, where the second day of operation was mostly dedicated to performing the visual inertial navigation and control experiments. The circumnavigation maneuver was not demonstrated successfully during the first test session. Data from this test showed higher than expected noise levels in the velocity measurement of the object through the stereo camera system. The higher noise levels coupled through controller gains ultimately resulting in firing times exceeding the maximum allotted time. The long firing times where, per design, scaled down to fit the allowable thrusting budget of the satellite, reducing the control authority of the force and torque control loops. Initially there was uncertainty to what the lighting conditions would be inside the JEM. The ability to measure and circumnavigate the object from ambient and artificial lighting had to be shown.

Similar to the numerical simulation test, the on-orbit experimental test was divided into three maneuvers, each ending after a pre-determined lap of time, and leading to the next one. From an operational point of view, the first maneuver, lasting ten seconds, consisted in letting both SPHERES in a free-floating mode upon being released in the test volume by the astronaut. Technically, the objective of the first maneuver was to let the state estimator converge from the acoustic metrology measurements. The estimated state vector was then used with feedback control – during the second maneuver – to set the inspector and object satellites in the respective initial conditions inside the test volume. Forty seconds was allotted for this initial positioning maneuver. The desired three-axis initial positions for each spacecraft, defined with respect to a coordinate reference frame attached to the ISS, are the same as those used in numerical simulations, i.e. $r_0 = [0.00 \ \ -0.68 \ \ 0.00]$ m and $r_0 = [0.00 \ \ 0.00 \ \ 0.00]$ m for the inspector and the target spacecraft respectively. Note that the origin of the coordinate reference frame system is located in the center of the test volume, which, as indicated in Table 3, also corresponds to the position of the geometric center of the target spacecraft for this experiment. The third maneuver started at 50 seconds into the test. Maneuver 3 would only last a few seconds and is used to initiate the spinning motion on the object satellite, if required. Maneuver 4 would last 300 seconds and performed the actual visual-inertial inspection trajectory.

Figure 10 shows four frames taken from actual footage during the test session experiment, on 12 March 2013. The first frame depicts both satellites at their respective initial position, with the inspector spacecraft being the one located closer to the ISS JEM camera (i.e. the spacecraft shown at the bottom of the first frame). The remaining three frames show the inspector spacecraft at different instant of its autonomous inspection trajectory. As qualitatively illustrated in Fig. 10, the inspector successfully demonstrated the ability to complete a fully-autonomous inspection trajectory around an unknown object in space using only a pair of stereo cameras and a gyroscope.

The ultrasound beacon-based navigation system described in Sec III provided the 3-axis position and velocity of the inspector which are plotted in Fig. 11 and Fig. 12. While the trajectory of the inspector satellite around the object was intended to remain in the *xy* plane, the actual trajectory has some noticeable motion in the *z* direction, as observed in Fig. 12. There has been some discussion as to the primary cause of this inclination, of which one or a combination of two ideas dominate. One probable cause is that the inspector satellite is not perfectly static or aligned with the *xy* plane at the beginning of the vision-based navigation and control maneuver (i.e. forth maneuver). This is clearly shown in the position history in Fig. 11, where at $t = 50$ seconds the desired initial position for the inspector is not perfectly reached. In other words, at the end of the initial positioning maneuver (second maneuver), the inspector spacecraft was still moving towards its desired initial position, as illustrated in the velocity plot in Fig. 12, introducing additional out of plane linear momentum. Furthermore, the inspector satellite would not be perfectly aligned in the inspectors roll frame. This initial misalignment would contribute to motion in the JEM perceived vertical direction. While it may seem that this problem can be avoided through increasing the time allotted for the initial positioning maneuver, it must be remembered that the position of the inspector satellite is subject to noise coupling from the acoustic ranging system and minimum firing time limitations on the satellite thrusters. All these factors contribute to constant no zero velocity of both the inspector and the object satellites.

Another source of error causing the off-plane motion might be due to a small mismatch in the expected and actual center of mass location, particularly in the *z* direction, which could have resulted in a non-ideal thrusting configuration scheme. Thrusting computations will not accommodate all thruster and mass variations in the system, as to always perfectly align the thrust vector with the center of mass of the satellite. Aspects such as CO_2 gas

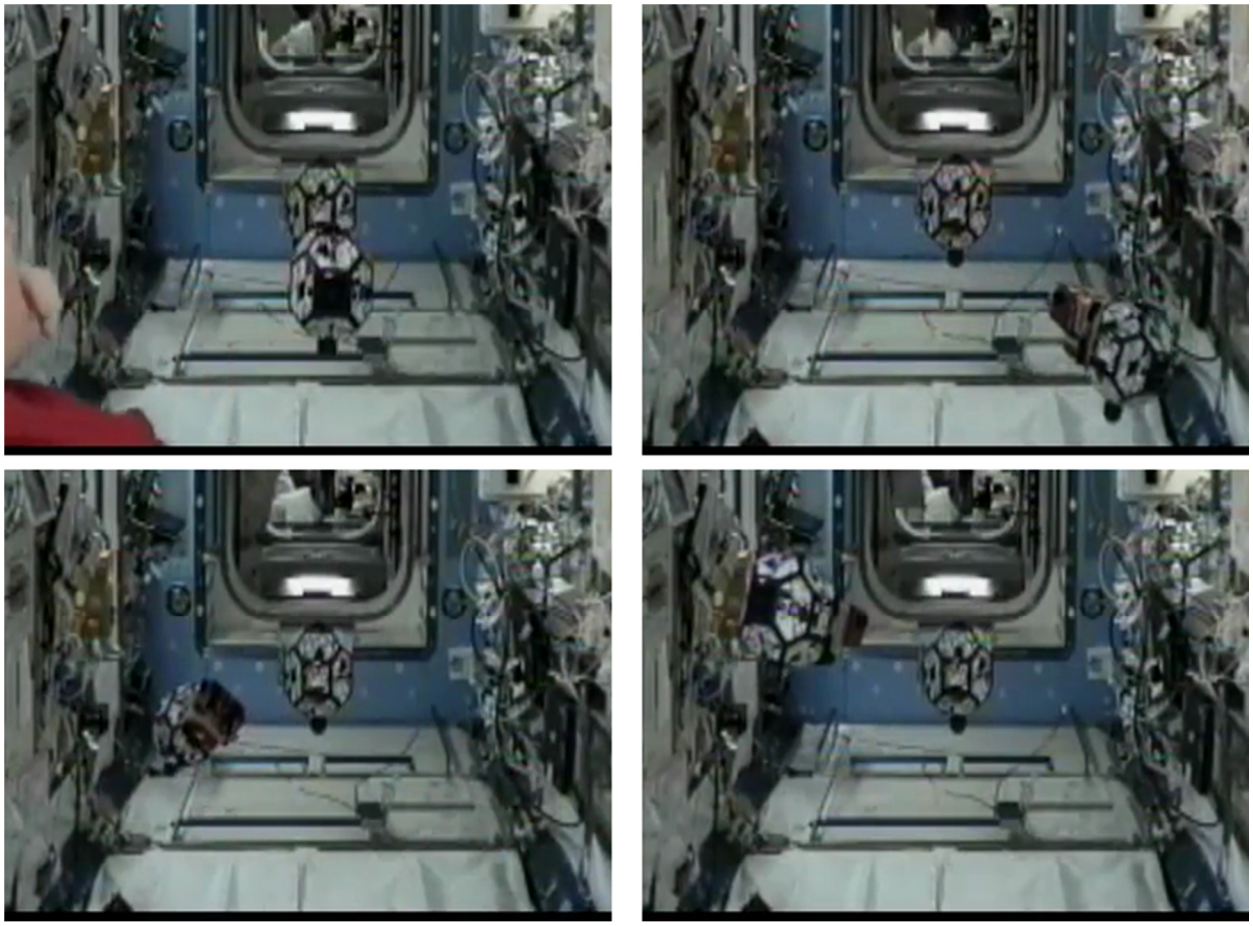

Fig. 10 On-orbit experimental results: autonomous vision-based inspection trajectory experiment aboard the ISS during Expedition 34.

expenditure are for example not considered. Therefore, during the initial acceleration phase, as the inspector satellite starts the circumnavigation maneuver, there will be large translational thrusting to transfer linear momentum in to the system. The expected *xy* navigation plane will therefore also be perturbed through the above mentioned errors.

The position of the inspector satellite over the course of the experiment is better visualized with the three-dimensional plot, provided in Fig. 11. This figure shows that despite the off-nominal motion along the *z* axis, the inspector successfully followed a circular trajectory with a relatively constant radius corresponding to the desired inspection distance of 0.68 m.

The top plot in Fig. 13 shows the range between the object and inspector satellites as the solid line. The range set-point during the visual-inertial circumnavigation maneuver is shown indicated by the dashed line. There is a clear hang-off error in relative range between the inspector and object. This constant range error, though relatively small, is attributed to insufficient feed forward translational thrust force. A few main factors may contribute to the reduced force. Firstly, lower than expected thruster performance from the CO2 thrusters. Note that the SPHERES satellite thrusters with a hand and gauge set gas regulator and the thrust scaling is furthermore taken as the mean performance over all thrusters of the three satellites which are on-orbit.

Secondly, part of this error may also be attributed to variation in vehicle mass. The circumnavigation test was run soon after a CO2 gas tank swap, whereby the mass of the satellite is above the mean mass of the vehicle, which is assumed to be at a half filled tank. While this hang-off error is not desirable, the error is comparatively small and the feedback system remains stable. Two other potential contributors to the hang-off errors have been considered. While the feedforward thrust term is computed by using the desired range and rotation rate, as described by Eq. (7), any variation in the line of sight vector to the center of the circumnavigation path would result in a projection of the required feed forward force opposing the centripetal acceleration acting on the inspector.

Lastly, the vision system tends to see more of the direct nearest surface of the object, rather than the slanted sides. Depending on lighting conditions, this would result in a biased range measurement to the object.

The rotation rates of the inspector satellite during the visual-inertial circumnavigation maneuver are an important indicator to the capability of the control law. The lower plot in Fig. 13 shows the yaw rotation rate of the inspector satellite. The roll and pitch rotation rate are omitted, as these values were stable around zero throughout the circumnavigation maneuver. Figure 13 illustrates some rotational motion during the first 50 seconds while the satellites are brought to their initial positions. At 50 seconds, the visual-inertial circumnavigation maneuver is initiated and the yaw rotation rate is ramped from zero to the desired yaw rate set-point of 1 degree per second. The ramp-up period was set to 15 seconds. The satellite followed closely the rotation rate ramp input command, but a rate oscillation in the order of 25% set point rate was observed for the remaining portion of the maneuver.

Notice a similar oscillation pattern on the inspector velocities, as shown in Fig. 12. This indicates that there is couping between the translational and rotational modes of the system via the visual-inertial measurements. The source of this coupling is again attributed to variation in thruster performance and non-perfect alignment of the forces and expected center of mass of the satellite. Furthermore, the suggested control architecture, as shown in Fig. 1, does not include any damping for the rotational rates of the inspector satellite. It is therefore suggested that an angular acceleration damping term be added to the controller to ensure that the above mentioned oscillations are actively suppressed.

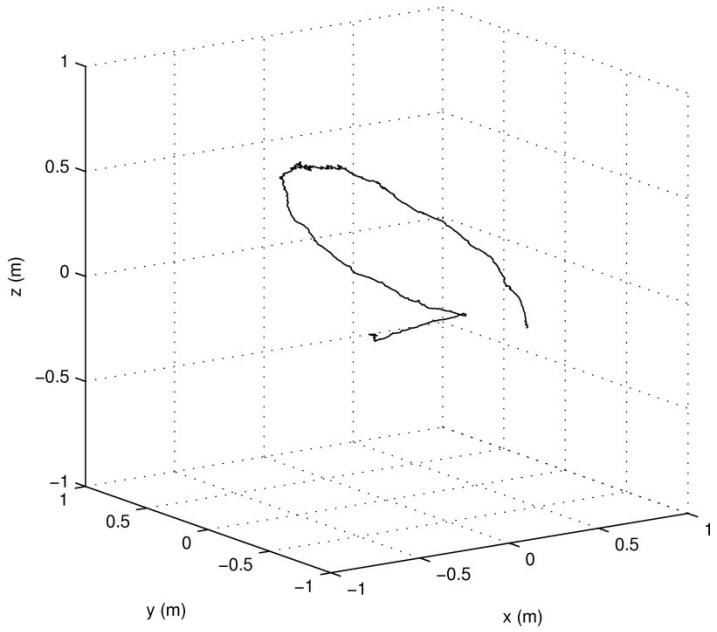

Fig. 11 On-orbit experimental results: 3D visualization of the inspector spacecraft circumnavigation trajectory.

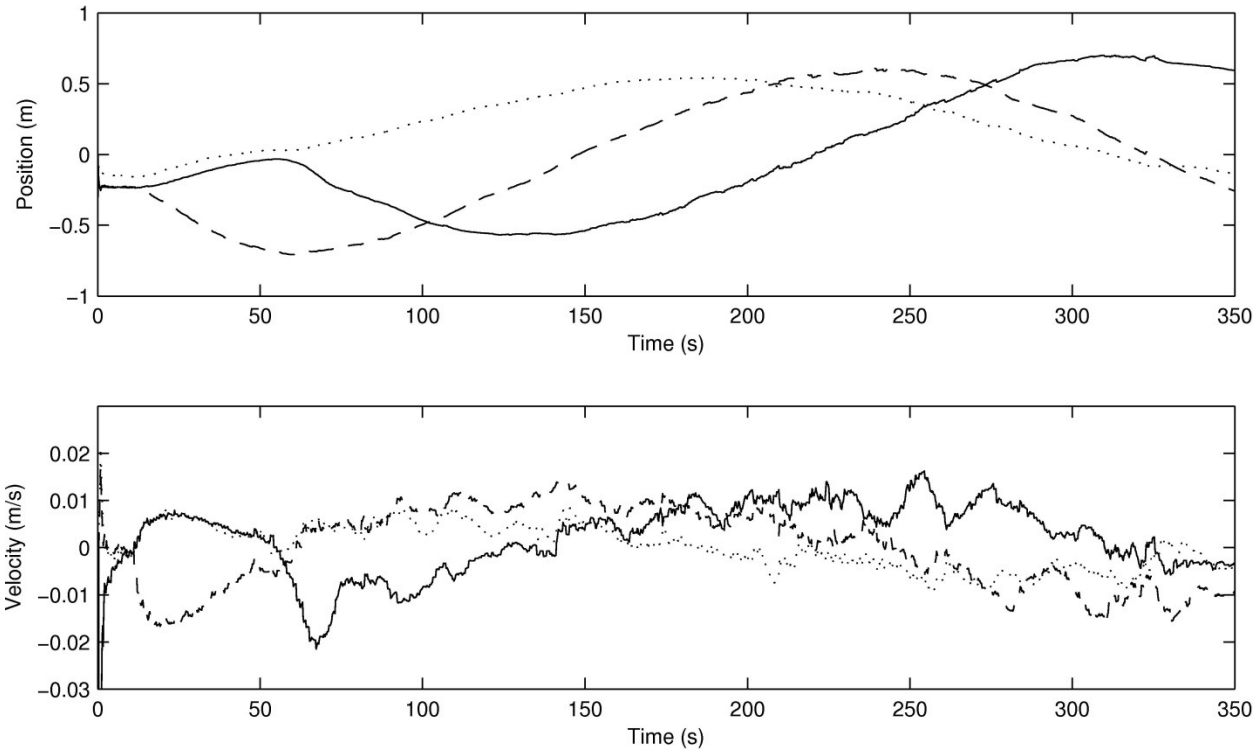

Fig. 12 On-orbit experimental results: inspector spacecraft position and velocity. The solid lines, the dashed lines and the dotted lines correspond to the *x*, *y* and *z* axis, respectively.

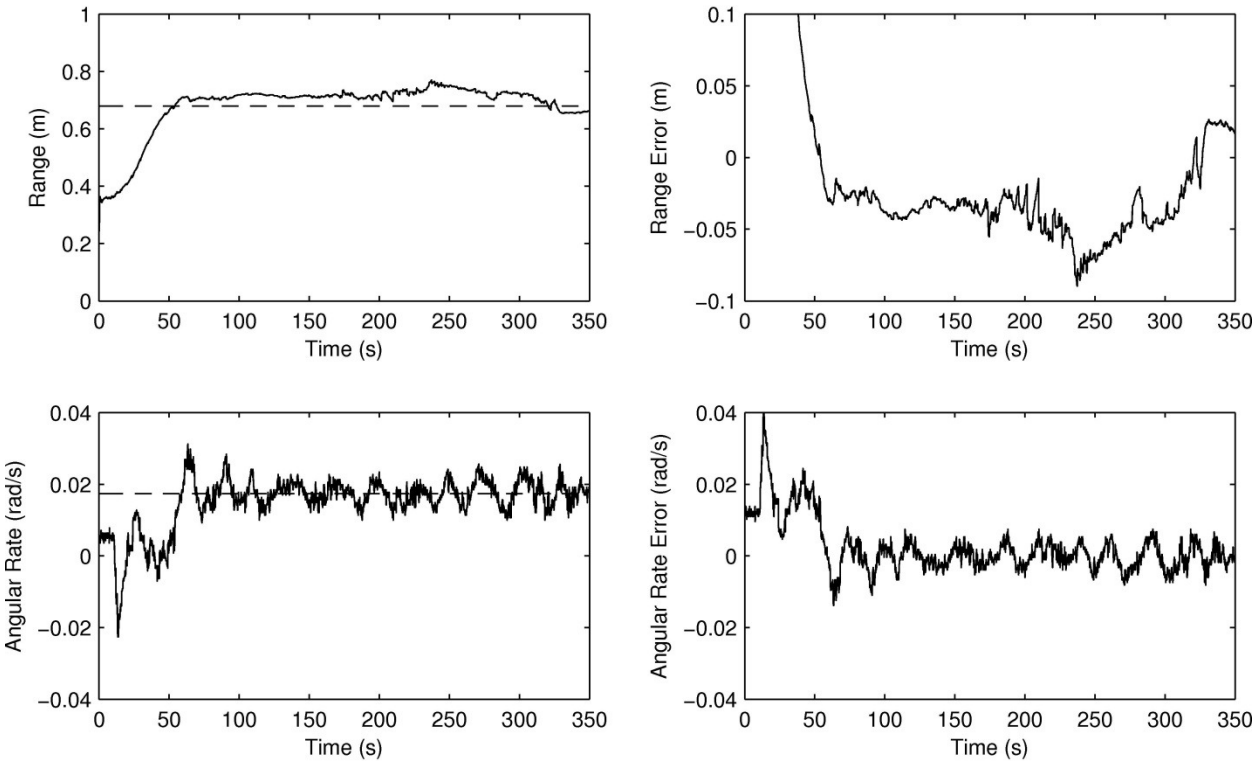

Fig. 13 On-orbit experimental results: range to target spacecraft and angular rate of the inspector spacecraft. The solid lines correspond to the actual values, and the dashed lines correspond to the desired values.

VIII. Conclusion

A comprehensive design and evaluation of an experiment on autonomous computer vision-based navigation and control as applied to the inspection of an unknown spacecraft has been conducted by the Space Systems Laboratory at the Massachusetts Institute of Technology in conjunction with Aurora Flight Sciences, the United States DoD Space Test Program, and NASA. The technology developed during the VERTIGO program and demonstrated during the ISS Expeditions 34 and 35 satisfied the first primary objective, which was to understand how to perform a relative circumnavigation inspection trajectory around an unknown object in space by relying solely on camera hardware and inertial sensors.

To enable research in vision-based navigation, a new hardware addition to the existing SPHERES, known as VERTIGO Goggles, was developed. The main hardware components of VERTIGO Goggles include a pair of monochrome stereo cameras, two illuminating LEDs, and a dedicated 1.2 GHz computer and power source.

It was shown that a reconfigurable thruster mapping strategy is required to accommodate, in real-time, variation in the mass distribution of the inspector satellite. This aspect is emphasized when the inspector satellite is expected to manipulate and interact with the object, as this would constantly vary the mass distribution of the satellite. Examples of this could include space debris collection or on-orbit servicing of satellites.

To aid the initial development and validate the proposed navigation and control methodology, numerical simulations were performed in a high-fidelity MATLAB simulation environment. Simulation results confirmed the feasibility the approach and demonstrated good performance in terms of relative position control. An on-orbit experiment demonstrated the successful completion of an autonomous circular inspection trajectory around an unknown object while maintaining a constant relative position between the two bodies.

This visual-inertial circumnavigation maneuver now allows for the collection of data which can be used to develop a visual and volumetric model of the unknown object. While algorithms to reconstruct a model of the object have already been demonstrated on the ground, the next step would be to incorporate these algorithms on the VERTIGO hardware for in-situ operation.

In conclusion, these results summarize a very successful investigation of the image processing, relative navigation and control design issues associated with a contemporary solution to the autonomous inspection of an unknown spacecraft problem. It is now hoped that these experimental on-orbit results will improve the confidence in these advanced technologies so that the developed tools can be applied to future spacecraft robotics missions.

Acknowledgments

The authors would like to acknowledge Professor John Leonard and Professor David W. Miller from the Massachusetts Institute of Technology for their support on the project. Furthermore, the authors would like to thank NASA Astronauts Tom Marshburn and Kevin Ford for having operated the VERTIGO experiment on the International Space Station during Expeditions 34 and 35. The authors are also very grateful to U.S. Department of Defence's Space Test Program, the human spaceflight office at NASA Johnson Space Center and the Marshall Space Flight Center payload operations team for their support of the operations. Special thanks go to Aurora Flight Sciences for their efforts in the development of the VERTIGO Goggles hardware. This research was funded by the Defense Advanced Research Projects Agency. Finally, Steve Ulrich also acknowledges the Natural Sciences and Engineering Research Council of Canada (NSERC) for their financial support under the Postdoctorate Fellowship Award PDF–438572–2013.

References

[1]Geller, D. K., "Orbital Rendezvous: When is Autonomy Required," *Journal of Guidance, Control, and Dynamics*, Vol. 30, No. 4, 2007, pp. 974–981.

[2]Lampariello, R., "Towards Semi-Autonomous Grasping of a Non-Cooperative Target," *IEEE International Conference on Robotics and Automation*, Inst. of Electrical and Electronics Engineers, Piscataway, NJ, May 2012.

[3]Hablani, H. B., "Autonomous Inertial Relative Navigation with Sight-Line-Stabilized Integrated Sensors for Spacecraft Rendezvous," *Journal of Guidance, Control, and Dynamics*, Vol. 32, No. 1, 2009, pp. 172–183.

[4]Tweddle, B. E., "Computer Vision Based Navigation for Spacecraft Proximity Operations," Master's thesis, Department of Aeronautics and Astronautics, Massachusetts Institute of Technology, 2010.

[5]Linares, R., Crassidis, J. L., and Cheng, Y., "Constrained Relative Attitude Determination for Two-Vehicle Formations," *Journal of Guidance, Control, and Dynamics*, Vol. 34, No. 2, 2011, pp. 543–553.

[6]Romano, M., Friedman, D. A., and Shay, T. J., "Laboratory Experimentation of Autonomous Spacecraft Approach and Docking to a Collaborative Target," *Journal of Spacecraft and Rockets*, Vol. 44, No. 1, 2007, pp. 164–173.

[7]Tweddle, B. E., "Relative Computer Vision Based Navigation for Small Inspection Spacecraft," *AIAA Guidance, Navigation, and Control Conference*, Portland, OR, August 2011.

[8]MacLean, S. G. and Pinkney, H. F. L., "Machine Vision in Space," *Canadian Aeronautics and Space Journal*, Vol. 29, No. 2, 1993, pp. 63–77.

[9]Howard, R., Heaton, A., Pinson, R., and Carrington, C., "Orbital Express Advanced Video Guidance Sensor," *IEEE Aerospace Conference*, Inst. of Electrical and Electronics Engineers, Piscataway, NJ, May 2008, pp. 1–10

[10]Henshaw, C. G., Healy, L., and Roderick, S., "LIIVe: A Small, Low-Cost Autonomous Inspection Vehicle," *AIAA SPACE 2009 Conference and Exposition*, Pasadena, CA, 2009.

[11]Tweddle, B. E., Saenz-Otero, A., and Miller, D. W., "Design and Development of a Visual Navigation Testbed for Spacecraft Proximity Operations," *AIAA SPACE Conference and Exposition*, Pasadena, CA, 2009.

[12]Nolet, S., "The SPHERES Navigation System: from Early Development to On-Orbit Testing," *AIAA Guidance, Navigation, and Control Conference*, Hilton Head, SC, Aug 2007.

[13]Mohan, S., "Quantitative Selection and Design of Model Generation Architectures for On-Orbit Autonomous Assembly," Ph.D. thesis, Department of Aeronautics and Astronautics, Massachusetts Institute of Technology, 2010.

[14]Cheng, Y., Maimone, M., and Matthies, L., "Visual Odometry on the Mars Exploration Rovers - A Tool to Ensure Accurate Driving and Science Imaging," *IEEE Robotics & Automation Magazine*, Vol. 13, No. 2, 2006, pp. 54–62.

[15]Nist´er, D., Naroditsky, O., and Bergen, J., "Visual odometry," *IEEE Computer Society Conference on Computer Vision and Pattern Recognition*, Washington, DC, June-July 2004.

[16]Scaramuzza, D., and Fraundorfer, F., "Visual Odometry," *IEEE Robotics & Automation Magazine*, Vol. 18, No. 4, pp. 80–92.

[17]Huang, A. S., Bachrach, A., Henry, P., Krainin, M., Maturana, D., Fox, D., and Roy, N., "Visual Odometry and Mapping for Autonomous Flight Using an RGB-D Camera," *International Symposium on Robotics Research*, Flagstaff, AZ, Sept. 2011.

[18]Bradski, G. and Kaehler, A., *Learning OpenCV: Computer Vision with the OpenCV Library*, O'Reilly, Cambridge, MA, 2008.

[19]Geiger, A., Roser, M., and Urtasun, R., "Efficient Large-Scale Stereo Matching," *Asian Conference on Computer Vision*, Queenstown, New Zealand, Nov. 2010.